Effect of aspect ratio of graphene oxide on properties of poly (vinyl alcohol) nanocomposites

Morimune-Moriya, Seira

Goto, Takuya

Nishino, Takashi

(Citation)
Nanocomposites,5(3):84-93

(Issue Date)
2019-08-14

(Resource Type)
journal article

(Version)
Version of Record

(URL)
https://hdl.handle.net/20.500.14094/90006447

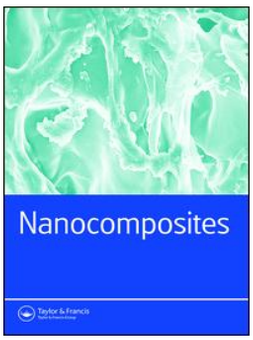

Nanocomposites

ISSN: 2055-0324 (Print) 2055-0332 (Online) Journal homepage: https://www.tandfonline.com/loi/ynan20

Effect of aspect ratio of graphene oxide on properties of poly (vinyl alcohol) nanocomposites

Seira Morimune-Moriya, Takuya Goto & Takashi Nishino

To cite this article: Seira Morimune-Moriya, Takuya Goto & Takashi Nishino (2019) Effect of aspect ratio of graphene oxide on properties of poly (vinyl alcohol) nanocomposites, Nanocomposites, 5:3, 84-93, DOI: 10.1080/20550324.2019.1647688

To link to this article: https://doi.org/10.1080/20550324.2019.1647688

Published online: 14 Aug 2019.

NANOCOMPOSITES
2019, VOL. 5, NO. 3, 84–93
https://doi.org/10.1080/20550324.2019.1647688

Taylor & Francis
Taylor & Francis Group

Effect of aspect ratio of graphene oxide on properties of poly (vinyl alcohol) nanocomposites

Seira Morimune-Moriya[a], Takuya Goto[b] and Takashi Nishino[c]

[a]Department of Applied Chemistry, College of Engineering, Chubu University, Kasugai, Japan; [b]Mitsubishi Gas Chemical Inc., Tokyo, Japan; [c]Department of Chemical Science and Engineering, Graduate School of Engineering, Kobe University, Kobe, Japan

ABSTRACT

In this study, the effect of aspect ratio of graphene oxide (GO) on the properties of poly (vinyl alcohol) (PVA) nanocomposites were investigated. The PVA/GO nanocomposites were prepared by a simple solution casting method. GO with 3 different lateral sizes, 0.5, 1.5 and 3 μm were used. The higher the aspect ratio, the higher the Young's modulus obtained. The effect of aspect ratio on Young's modulus was in agreement with the Halpin-Tsai model, especially when GO was highly aligned in uniaxially drawn nanocomposites. Similar to the Young's modulus, the barrier properties increased with increasing GO aspect ratio. On the other hand, the highest glass transition temperature as well as the highest thermal decomposition temperature was achieved for the GO of the lowest aspect ratio.

GRAPHICAL ABSTRACT

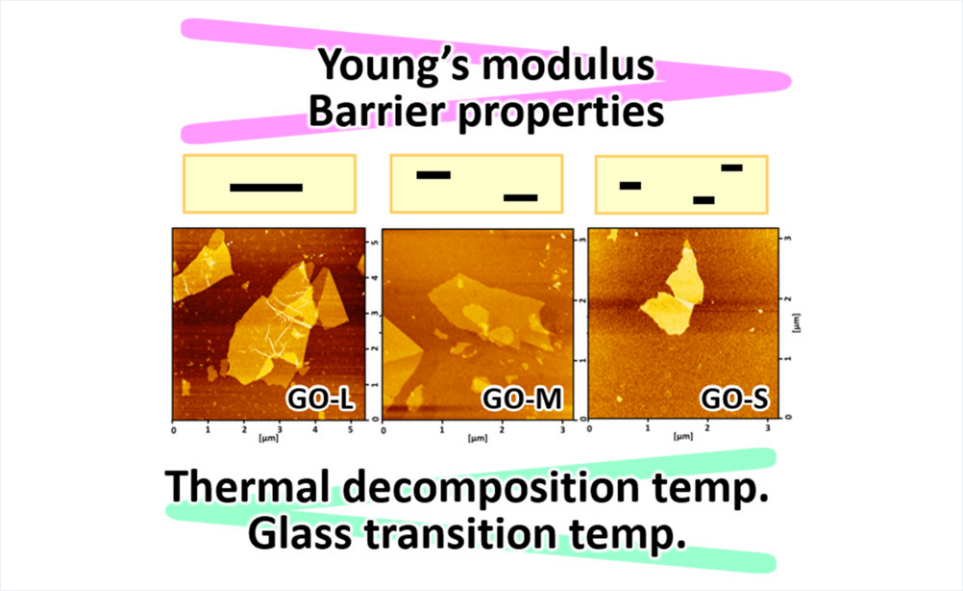

ARTICLE HISTORY
Received 27 April 2019
Accepted 20 July 2019

KEYWORDS
Graphene oxide; poly (vinyl alcohol); aspect ratio; mechanical properties; thermal properties; barrier properties; reinforcement effect

1. Introduction

In recent years, two-dimensional graphene composed of sp^2-bonded carbon atoms has been one of the most attractive materials in nanotechnology in view of the excellent properties, such as the Young's modulus of 1 TPa and ultimate strength of 130 GPa [1], thermal conductivity of 5000 W/mK [2], and electrical conductivity of 6000 S/cm [3]. Graphene has been synthesized either by bottom-up processes, such as epitaxial growth on single-crystal SiC [4], or top-down processes of separation/exfoliation of graphite or graphite derivatives [5, 6]. Due to the high availability and low cost of graphite, top-down processes starting from graphite have often been used. Hummers method [7] is one of the most widely known top-down processes of graphene. Graphene oxide (GO) has been obtained through the process of Hummers method [8, 9]. Several oxygen containing functional groups, such as hydroxyl, carbonyl, carboxyl and epoxy groups, on the surface

CONTACT Takashi Nishino tnishino@kobe-u.ac.jp Department of Chemical Science and Engineering, Graduate School of Engineering, Kobe University, Rokko, Nada, Kobe 657-8501, Japan

of GO enable GO to exfoliate in water or other protic solvents [10, 11]. So far, many works have been conducted on GO reinforced polymer nanocomposites and improvements in mechanical properties have been reported [12–18].

Previously, we have used poly (vinyl alcohol) (PVA), which is well-known as a water-soluble polymer, as a matrix for GO reinforced polymer nanocomposites [13, 14]. The PVA/GO nanocomposites were prepared by a simple casting of a PVA/GO aqueous suspension. GO was dispersed at the nanoscale in PVA matrix with strong interactions between filler and matrix, mainly by hydrogen bonding. As a result, the nanocomposites showed remarkable enhancement in their properties even at a small amount of GO up to 1% w/w. For example, the Young's modulus and tensile strength increased by 100% and 45%, respectively, with only 1% w/w GO loading. Poly (methyl methacrylate) (PMMA), a hydrophobic polymer, was also used as a matrix for GO reinforced nanocomposites [15]. The PMMA/GO nanocomposites were also prepared using water as a processing medium. In the mechanical tensile tests, GO played a role in the crack pinning for the nanocomposites. Therefore, the elongation at break of PMMA was maintained and the nanocomposite showed the remarkable increase in toughness. Besides, the thermal decomposition temperature of the nanocomposite was increased by 28 °C with only 1% w/w GO. Furthermore, the barrier properties of the nanocomposite with 10% w/w GO was found to be almost impermeable.

The properties of polymer composites depend on several factors, such as dispersibility of fillers, interface adhesion and morphology of fillers [19, 20]. Sumita et al. [21] conducted the research on the size effect of filler of nylon 6 composites filled with ultrafine and micron-sized silica particles. They showed that the nanocomposites reinforced by nano-sized silica particles exhibited higher rigidity and superior yield strength compared to the composites reinforced by micron-sized silica particles. Nanocomposites have often achieved superior properties over macro or micro sized filler reinforced composite because of the large specific surface area, short interparticle distance and so on [22, 23]. It is well-known that not only the size but also the aspect ratio of fillers has a large effect on properties of composites as shown in the Halpin-Tsai model [24]. There are several reports conducted on the effect of aspect ratio of clays, graphene and carbon nanotube on properties of polymer composites [25–33]. For example, Weon et al. [25] investigated the effect of aspect ratio and orientation of clay on properties of nylon-6 nanocomposites. It was revealed that higher aspect ratio and unidirectional orientation of clay resulted in significant increase in the Young's modulus, tensile strength and heat distortion temperature of the nanocomposites. In addition to the effect of aspect ratio, that of surface functionality of graphene nanoplatelets (GNPs) on mechanical properties were reported by Chong et al. [32] They showed that the reinforcement effect of GNPs significantly decreased by agglomeration due to the reduced aspect ratio. It was obvious that, in order to discuss the effect of aspect ratio on the properties of the nanocomposites, high dispersibility and favorable interactions should be achieved. In this study, we prepared PVA/GO nanocomposites with three different-sized GO. The effect of aspect ratio of GO on the properties of the nanocomposites were investigated.

2. Experimental

2.1. Materials

GO aqueous suspensions (1% w/w) with three different-sized GO were supplied by Mitsubishi Gas Chemical. Inc. (Tokyo, Japan). NanoGRAX, NanoGRAX-1 and NanoGRAX-2 refer to the aqueous suspensions of GO with average size of 3, 1.5 and 0.5 μm, respectively, according to the manufacturer. The size of GO was controlled by ultrasonication. The PVA powder "Gohsenol NH-18" was supplied from Nippon Synthetic Chemical Industry Co., Ltd. (Osaka Japan). The degree of polymerization was 1800, and the degree of saponification was higher than 99%.

2.2. Sample preparation

The PVA powder was dissolved in water at 90 °C. The PVA solution (5% w/w) and the GO aqueous suspension (1% w/w) were mixed together under stirring for 1 day. The homogeneous suspension of PVA/GO was cast into a petri dish and dried at room temperature followed by vacuum drying at 40 °C for 48 h [13]. The uniaxially drawn nanocomposites were prepared by drawing the as-cast nanocomposite films in an oven at 160 °C to draw ratio of 3, which was the maximum draw ratio [14].

2.3. Characterization

The atomic force microscopic (AFM) analysis was performed in tapping mode with a silicon cantilever probe (NanoNavi Station/E-sweep, Seiko Instruments Inc., Chiba, Japan). The sample was prepared by spin-coating of diluted GO aqueous suspension on a silicon wafer.

A field emission scanning electron microscope (FE-SEM) (JEOL, JSM-6700F) was used at an

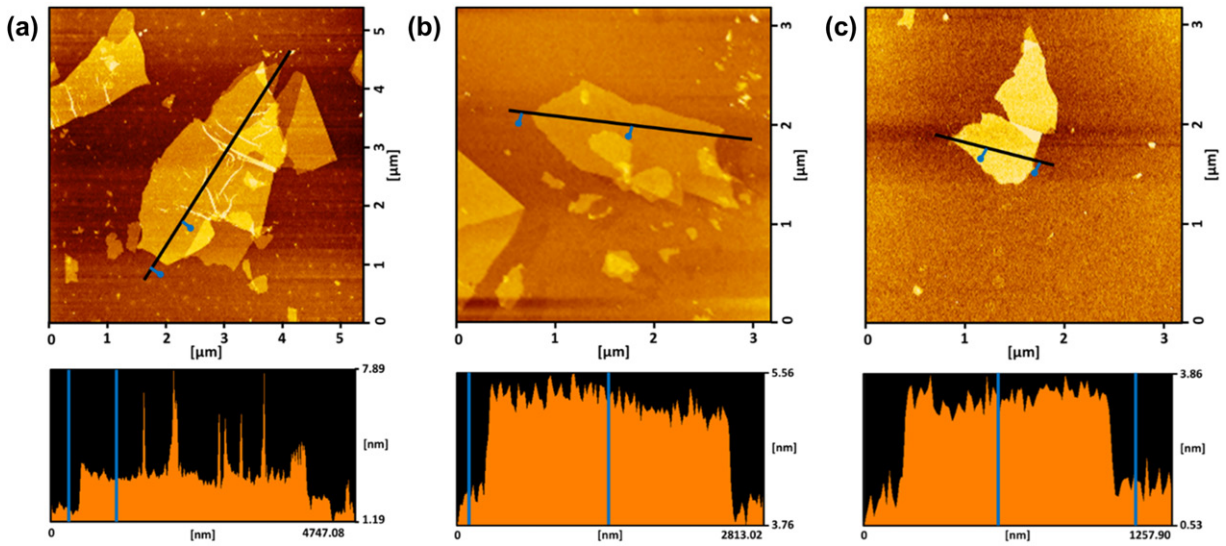

Figure 1. AFM height images and height profiles of (a) GO-L, (b) GO-M and (c) GO-S.

accelerating voltage of 10 kV. The cross sections of PVA/GO nanocomposites were observed. X-ray diffraction was carried out with an X-ray diffractometer (RINT2100, Rigaku, Tokyo, Japan). The Ni-filtered CuKα radiation beam was operated at 40 kV and 20 mA. The scanning speed was 1.0 degree/min and the $2\theta/\theta$ scan data were collected at 0.02 degree intervals. The crystallinity (X_c) of PVA was determined using the following equation:

$$Xc = \frac{Ac}{(Ac + Aa)} \times 100 \quad (1)$$

where Ac is the area of the crystalline regions and Aa is the area of the amorphous region.

The mechanical properties of the nanocomposites were measured using a tensile tester (Autograph AGS-1kND, Shimadzu Co., Kyoto, Japan). The initial length of the specimen was 20 mm, and the crosshead speed was 2 mm/min. More than ten specimens were tested. The toughness (K), which is defined as the area surrounded by the stress (σ)–strain (ε) curve, was calculated using the following equation:

$$K = \int_{\varepsilon=0}^{\varepsilon=\varepsilon_{\max}} \sigma \cdot d\varepsilon/\rho\,(\mathrm{J/g}) \quad (2)$$

where σ is stress (Pa), ε is strain (%) and ρ is density (g/m^3). The density was determined by floatation using tetrachloride (1.5842 g/cm^3) and benzene (0.88 g/cm^3) at 30 °C. Fragments of films were placed in the mixture and allowed to settle for 2 days. The volume of the pycnometer was calibrated with distilled water (0.99565 g/cm^3).

The swelling ratio was measured by immersing the square specimens (2 cm × 2 cm) in distilled water (30 °C). The swelling ratio was defined as the weight gain of the specimens by using the equation as follows:

$$\text{Swelling ratio} = \left(\frac{W}{W0}\right) \quad (3)$$

where, W_0 and W are the weight of the specimen before and after swelling, respectively. The weight of the specimens was measured every 10 min for the first 60 min and every 30 min for the rest. The specimens were immersed in water for 300 min in total till they reach the equilibrium of swelling. The diffusion coefficient of water (D) was calculated using the following equation [34]:

$$D = \pi\left(\frac{Qr}{4}\right)^2 (\mathrm{m^2/s}) \quad (4)$$

where Q is the slope of the linear approximation obtained by plotting the swelling ratio versus the square root of the swelling time and r is the thickness of the specimens.

Thermal decomposition temperature (T_d) was measured by a thermogravimeter (TG) (TG/DTA-220CU, Seiko Instruments Inc., Chiba, Japan) under nitrogen flow with a heating rate of 10 °C/min. T_d was defined as a temperature of 5% w/w thermal weight loss. Dynamic mechanical analysis (DMA) was performed by a dynamic mechanical analyser (DVA-220S, ITK Co., Ltd., Osaka, Japan) under nitrogen flow. A heating rate of 6 °C/min was employed with a frequency of 10 Hz.

3. Results and discussion

3.1. Morphology of GO

Figure 1a–c shows the AFM height images and the height profiles of three kinds of GO sheets. The GO with average size of 3, 1.5 and 0.5 μm was termed as GO-L, GO-Mand GO-S, respectively. In addition to the size-controlled GO, some fragments were observed

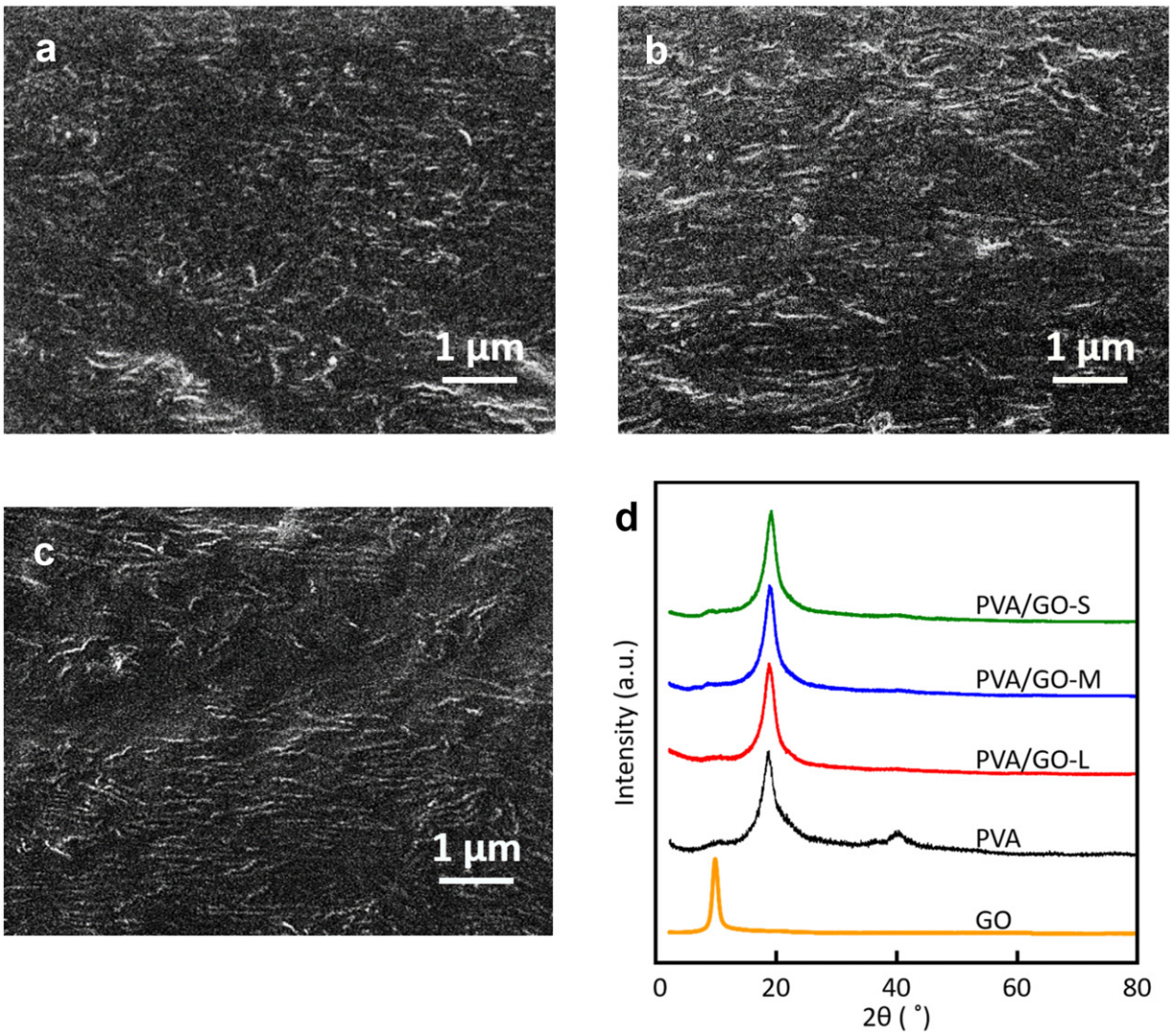

Figure 2. SEM images of (a) PVA/GO-S nanocomposite, (b) PVA/GO-M nanocomposite and (c) PVA/GO-L nanocomposite (GO content = 1% w/w); (d) X-ray diffraction profiles of GO, PVA and PVA/GO nanocomposites (GO content = 1% w/w).

for all the samples. Judging from the height profiles, the average thickness was 1.0 ± 0.5 nm in all cases.

3.2. Structure of PVA/GO nanocomposites

Figure 2a–c show the SEM images of the cross sections of the PVA/GO nanocomposites with 1% w/w GO loading. It was revealed that GO sheets, observed as light lines, were homogeneously dispersed in PVA for all the nanocomposites. Figure 2d shows the X-ray diffraction profiles of the PVA and PVA/GO nanocomposites with 1% w/w GO loading. The X_c of the nanocomposites were higher (35%) than that of neat PVA (28%). There was no significant difference in X_c with respect to the aspect ratio of GO.

3.3. Mechanical properties of PVA/GO nanocomposites

So far, a number of micro-mechanical composite models have been proposed to describe the macroscopic mechanical properties of composites [24, 25, 35, 36]. Among them, the Halpin-Tsai model [24] or the modified Halpin-Tsai model [16,37,38] (Equations (5)–(10)) have widely been used for the estimation of Young's modulus:

$$E_{c//} = \frac{1 + \xi\eta_L V_f}{1 - \eta_L V_f} E_m \quad (5)$$

$$E_{c\perp} = \frac{1 + 2\eta_T V_f}{1 - \eta_T V_f} E_m \quad (6)$$

$$E_{cR} = \frac{3}{8}E_{c//} + \frac{5}{8}E_{c\perp} = \left(\frac{3}{8}\frac{1 + \xi\eta_L V_f}{1 - \eta_L V_f} + \frac{5}{8}\frac{1 + 2\eta_T V_f}{1 - \eta_T V_f}\right)E_m \quad (7)$$

$$\eta_L = \frac{\frac{E_f}{E_m} - 1}{\frac{E_f}{E_m} + \xi} \quad (8)$$

$$\eta_T = \frac{\frac{E_f}{E_m} - 1}{\frac{E_f}{E_m} + 2} \quad (9)$$

where $E_{c//}$, $E_{c\perp}$, and E_{cR} are Young's modulus of a composite with fillers oriented parallel,

perpendicular and random with the loading direction, respectively. E_f and E_m are Young's modulus of fillers and matrix, respectively. V_f, is volume fraction of fillers. ξ depends on morphology of fillers and is given by Equation (10) for 2D platelet fillers [16, 37]:

$$\xi = \frac{2}{3}\alpha_f = \frac{2}{3}\frac{l_f}{t_f} \quad (10)$$

where α_f is the maximum aspect ratio of fillers. This model clearly shows that the aspect ratio is one of the important factors for the enhancement of mechanical properties of nanocomposites.

Figure 3a–c shows the stress-strain curves of PVA and PVA/GO nanocomposites. The Young's modulus, tensile strength, elongation at break and toughness obtained from these curves were shown in Figure 3d–g. It is obvious from the data that the aspect ratio of GO affects the Young's modulus of the nanocomposites. The higher the aspect ratio, the higher the Young's modulus of the nanocomposites. The effect of aspect ratio was clearly apparent in the Young's modulus of uniaxially drawn nanocomposites with 1% w/w GO, where GO sheets were highly oriented parallel to the film surface [14]. From the Halpin-Tsai model, the $E_{c//}$ of the uniaxially drawn PVA/GO-S nanocomposite is 10% higher than that of PVA/GO-L nanocomposite when the filler content is 1% w/w. As shown in Figure 3h, The Young's modulus of PVA/GO-L (18.3 GPa) was 11% higher than that of PVA/GO-S (16.6 GPa) for the uniaxially drawn nanocomposites, which was in good agreement with the Halpin-Tsai model. The aspect ratio didn't affect the tensile strength of the as-cast isotropic nanocomposites while that of the uniaxially drawn nanocomposites with low content less than 0.5 wt% showed a similar trend to the Young's modulus (Figure 3i). It was assumed that the orientation of GO significantly enhanced the effect of the aspect ratio on the tensile strength of the nanocomposites. The reason of the decrease in the tensile strength of the uniaxially drawn nanocomposites with 1% w/w GO-L can be explained by the embrittlement as mentioned below.

The reinforcement effect of rigid fillers on polymers can predict from the ratio of the Young's modulus of composites and matrix, E_c and E_m, respectively [38]. This approach was introduced by Halpin and Thomas [39] and the equation is given as follows:

$$\frac{E_c}{E_m} = \frac{1 + \xi\eta_L V_f}{1 - \eta_L V_f} \quad (11)$$

Gao et al. [33] reported the effect of filler size on the properties of poly (lactide acid) (PLA) by using two kinds of GNPs, GNP-S and GNP-L with aspect ratio of ~500 and ~2000, respectively. The PLA/GNP-L composites showed higher Young's modulus and tensile strength than those of PLA/GNP-S composites. It was revealed that the E_c/E_m of the both nanocomposites exhibited linear increase and in agreement with mechanical models. On the other hand, in this study, the nanocomposites with GO-S showed higher E_c/E_m than the theoretical values while the experimental data well fitted with the theoretical curve for the nanocomposites with high aspect ratio GO as shown in Figure 3j. The similar trend was observed for the nanocomposites with other GO content. It was assumed that the interfacial interaction between PVA and GO, the alignment of GO and the changes in the PVA molecular motion by GO enhanced the reinforcement effect and further improved the mechanical properties of the nanocomposites [16, 17, 32].

Interestingly, the elongation at break value of the PVA/GO-L nanocomposites was lower than that of other GO composites for all GO contents. Therefore, the highest toughness was obtained for GO-L, which had the lowest aspect ratio. The increase in toughness by the low aspect ratio filler can be explained by the release of the strain energy and the crack pinning [40–43]. Wang et al. [42] investigated the fracture toughness of epoxy nanocomposites with highly exfoliated clay. They revealed that the presence of the nanoclay lead the crack propagation along a very tortuous path, forming many crazes in the nanocomposites. The formation of multiple crazes helps to release the strain energy, which is the major toughening mechanism in the nanocomposites. Su et al. [43] measured the critical energy release rate for the separation of the interface in polystyrene/gold nanoparticles nanocomposites. They revealed that the nanoparticles prevented lateral load transfer, therefore, effectively interfered with crack propagation. Since the number of particles in GO-S was three times larger than that in GO-L, GO-S, which could produce more crazes than GO-L, resulting in the effective release of the strain energy together with the crack pinning in the nanocomposites.

3.4. Thermal properties of PVA/GO nanocomposites

Figure 4a–c shows the thermogravimetric traces of PVA and PVA/GO nanocomposites. The 5% weight loss was determined as thermal decomposition temperature (T_d). Figure 4d and e show the T_d and the glass transition temperature (T_g) of PVA and PVA/GO nanocomposites, respectively. Both T_d and T_g increased by the incorporation of GO for almost all the nanocomposites. In general, there were two

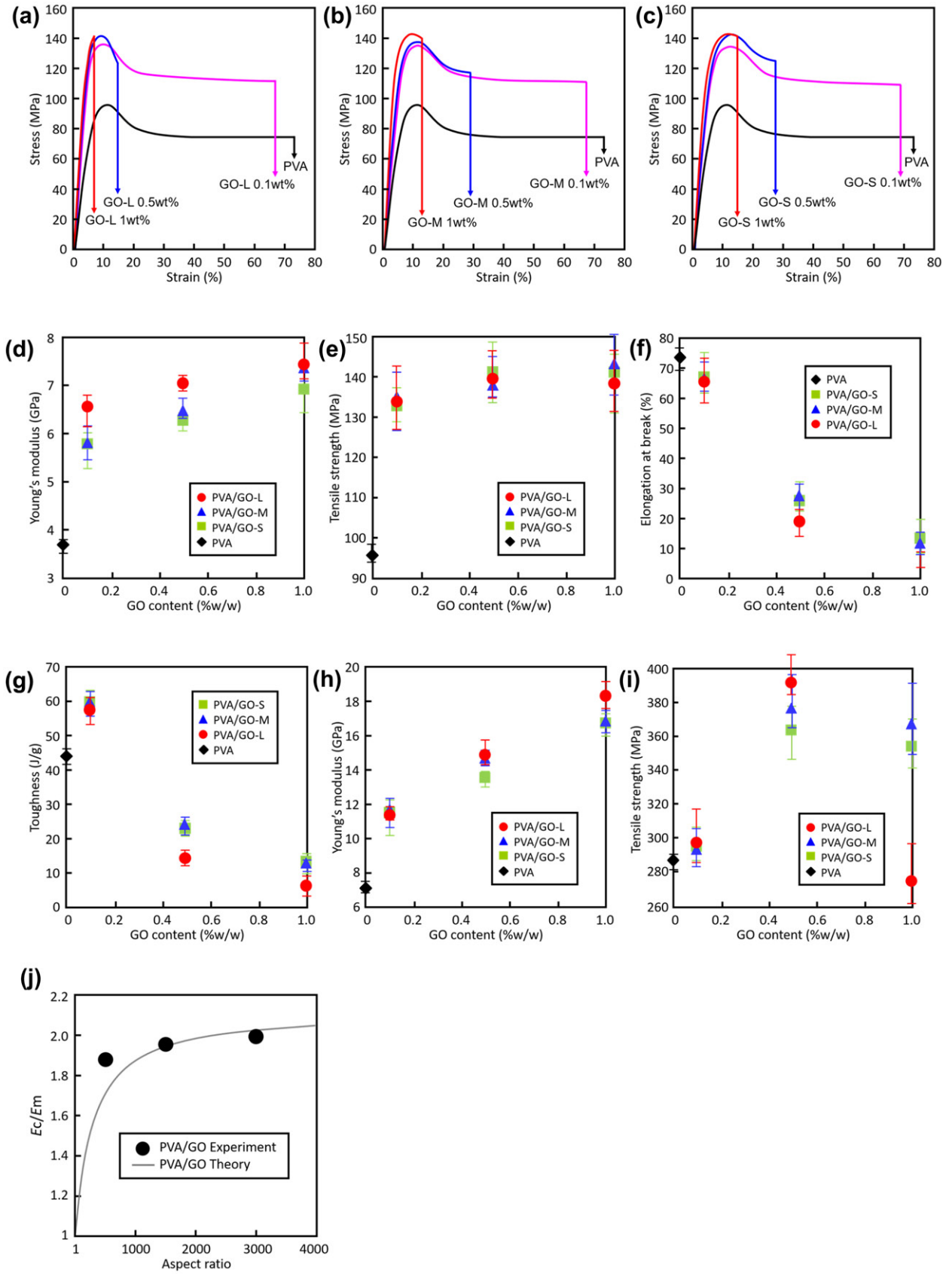

Figure 3. Stress–strain curves of PVA and (a) PVA/GO-L nanocomposites, (b) PVA/GO-M nanocomposites and (c) PVA/GO-S nanocomposites; (d) Young's modulus, (e) tensile strength, (f) elongation at break and (g) toughness of PVA and PVA/GO nanocomposites; (h) Young's modulus and (i) tensile strength of uniaxially drawn (×3) PVA and PVA/GO nanocomposites; (j) Theoretical fit using Equation (11) of PVA/GO nanocomposites (1 wt%).

reasons for the increase in T_d and T_g. First, GO significantly restricted the PVA molecular motion and prevented decomposition [12, 28–33]. Second, GO hindered the diffusion of the volatile products generated during the decomposition [12, 28, 29]. Among the PVA/GO nanocomposites, the

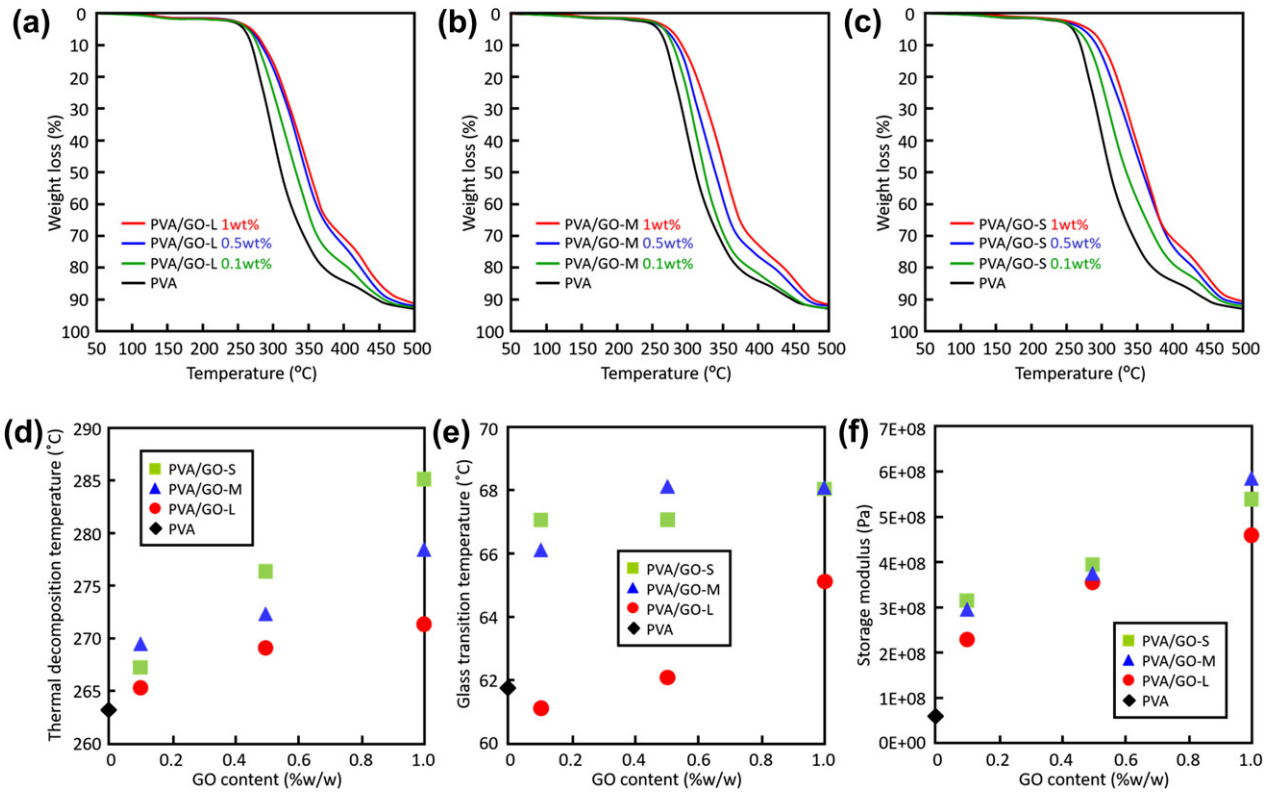

Figure 4. Thermogravimetric traces of PVA and (a) PVA/GO-L nanocomposites, (b) PVA/GO-M nanocomposites and (c) PVA/GO-S nanocomposites; (d) Thermal decomposition temperature (T_d) and (e) glass transition temperature (T_g) of PVA and PVA/GO nanocomposites; (f) Storage modulus of PVA and PVA/GO nanocomposites at 92 °C.

nanocomposites with GO-S showed the highest T_d and T_g. The storage modulus at the temperature above T_g is often used to estimate the apparent crosslink densities of the polymer networks [44]. As shown in Figure 4c, the storage modulus at 93 °C (30 °C above the T_g) showed similar behavior to those of T_d and T_g. This indicates that the interfacial interactions between PVA and GO were larger for the lower aspect ratio filler because of the higher specific surface area.

3.5. Barrier properties of PVA/GO nanocomposites

In general, the improved barrier properties of composites have been explained by 'torturous path' effect [45, 46]. The diffusion path length of molecules was increased due to the impervious fillers. It is well-known that the aspect ratio as well as the size of the filler have a large effect on barrier properties of polymer composites [47]. The high barrier properties have often been reported for the composites reinforced with 2D fillers with high aspect ratio such as clays and graphene [48–50]. Figure 5a–c shows swelling ratio of (a) PVA/GO-L (b) PVA/GO-M and (c) PVA/GO-S nanocomposites. Diffusion coefficient of water obtained from swelling ratio curves of as-cast and uniaxially drawn (×3) nanocomposites were shown in Figure 5d and e, respectively. The nanocomposites with GO-L showed the highest barrier properties. It was suggested that the presence of GO with high aspect ratio forced the tortuous pathway of water and effectively suppressed the diffusion of water in the nanocomposites.

The Nielsen model [51] and Cussler model [52] were applied to as-cast nanocomposites and uniaxially drawn nanocomposites, respectively. The Nielsen model is suitable for the composites where fillers are randomly oriented and given in Equation (12):

$$\frac{P_c}{P_m} = \frac{1 - V_f}{1 + \left(\frac{\alpha_f}{2}\right) V_f} \quad 12$$

where P_c and P_m are the permeability of composite and matrix, respectively. On the other hand, the Cussler model is applicable for the composites with highly aligned fillers and given as follows:

$$\frac{P_c}{P_m} = \left(1 + \frac{\alpha^2 {V_f}^2}{1 - V_f}\right)^{-1} \quad 13$$

As shown in Figure 5d, e, the nanocomposites with high aspect ratio at high content, especially for uniaxially drawn nanocomposites, showed good agreement with the theoretical values. However, there was a large divergence between the experimental results of the nanocomposites with low aspect ratio GO at low content and the theoretical values.

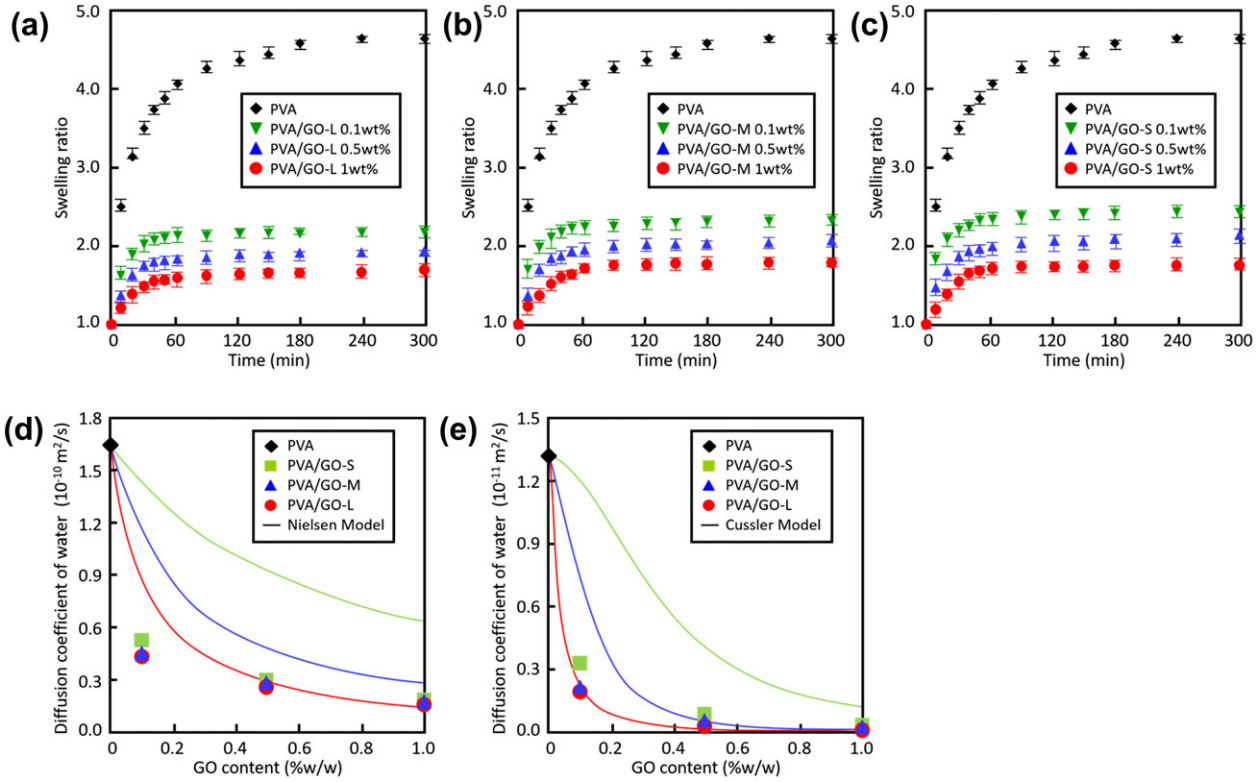

Figure 5. Swelling ratio of PVA and (a) PVA/GO-L nanocomposites, (b) PVA/GO-M nanocomposites and (c) PVA/GO-S nanocomposites; Diffusion coefficient of water of (d) as-cast and (e) uniaxially drawn (×3) PVA and PVA/GO nanocomposites.

It was assumed that such a high barrier effect at low content of GO was achieved by the confinement of the polymer chains [49, 50, 53]. Since GO highly dispersed in PVA and there were strong interfacial interactions between PVA and GO, the rigidification of PVA chains by GO could be strong. As shown above in thermal properties, it was assumed that GO-S restricted the molecular motion more effectively than GO-L. Therefore, incorporation of GO with low aspect ratio resulted in the significant drop of diffusion coefficient of water of the nanocomposites. The similar effect has also been suggested for clay reinforced nanocomposites [54–56]. It was obvious that the platelet morphology and large specific surface area of clays reduced the permeability by prolonging the penetration pathway of gas molecules more effectively than low aspect ratio fillers. In addition, clays could restrict the molecular motion of polymer chains and the compactness of the polymer networks increased for the composites. Therefore, the impenetrable crystalline domains of the polymers, which reduced the free volume for penetrating gas molecules, increased by the incorporation of clays, resulted in the high gas barrier properties of the composites.

4. Conclusions

The effects of GO aspect ratio on the mechanical, thermal and barrier properties of PVA/GO nanocomposites were investigated. Young's modulus increased with filler aspect ratio. The effect of aspect ratio on the Young's modulus was in agreement with Halpin-Tsai predictions when GO was highly aligned in uniaxially drawn nanocomposites. On the contrary, the elongation at break as well as toughness was increased with decreasing of the aspect ratio. It was suggested that GO with the lowest aspect ratio released the strain energy more effectively than other GO's. In terms of the thermal properties, the nanocomposites with GO-S achieved the highest T_g and T_d. It was suggested that the molecular mobility of the PVA matrix was restricted by GO-S more effectively than GO-L because of the high specific surface area. The high barrier properties against water was exhibited by the nanocomposites with GO of high aspect ratio due to the tortuous pathway. The low aspect ratio GO also showed the high barrier properties which may be dominated by the strong restriction of the PVA molecular motion.

Disclosure statement

No potential conflict of interest was reported by the authors.

Notes on contributors

Seira Morimune-Moriya is a senior assistant professor in department of applied chemistry at Chubu University. She has published on the structure and properties of polymer nanocomposites.

Takuya Goto is a researcher at Mitsubishi Gas Chem. Inc. He has worked on nanocarbon materials and its applications.

Takashi Nishino is a professor in department of chemical science and engineering at Kobe University. He has published on the structure and mechanical properties of polymers and nanocomposites, interface interaction between matrix and filler, and adhesion of polymers.

References

1. Lee C, Wei X, Kysar JW. Measurement of the elastic properties and intrinsic strength of monolayer graphene. Science. 2008;321:385–388.
2. Balandin AA, Ghosh S, Bao W, et al. Superior thermal conductivity of single-layer graphene. Nano Lett. 2008;8:902–907.
3. Du X, Skachko I, Barker A, et al. Approaching Ballistic Transport in Suspended Graphene. Nat Nanotechnol. 2008;3:491–495.
4. Berger C, Song Z, Li X, et al. Electronic confinement and coherence in patterned epitaxial graphene. Science. 2006; 312:1191–1196.
5. Dikin DA, Stankovich S, Zimney EJ, et al. Preparation and characterization of graphene oxide paper. Nature. 2007;448:457–460.
6. Sadak O, Sundramoorthy AK, Gunasekaran S. Facile and green synthesis of highly conducting graphene paper. Carbon. 2018;138:108–117.
7. Hummers WS, Offeman RE. Preparation of graphitic oxide. J Am Chem Soc. 1958;80:1339–1339.
8. Becerril HA, Mao J, Liu Z, et al. Evaluation of solution-processed reduced graphene oxide films as transparent conductors. ACS Nano. 2008;2:463–470.
9. Yang D, Velamakanni A, Bozoklu G, et al. Chemical analysis of graphene oxide films after heat and chemical treatments by X-ray photoelectron and micro-Raman spectroscopy. Carbon. 2009;47: 145–152.
10. Rourke JP, Pandey PA, Moore JJ, et al. The real graphene oxide revealed: stripping the oxidative debris from the graphene-like sheets. Angew Chem Int Ed. 2011;50:3173–3177.
11. Wen X, Garland CW, Hwa T, et al. Crumpled and collapsed con- formations in graphite oxide membranes. Nature. 1992;355:426–428.
12. Kim H, Abdala AA, Macosko WC. Graphene/polymer nanocomposites. Macromolecules. 2010;43: 6515–6530.
13. Morimune S, Nishino T, Goto T. Poly (vinyl alcohol)/graphene oxide nanocomposites prepared by a simple eco-process. Polym J. 2012;44:1056–1063.
14. Morimune S, Kotera M, Nishino T, et al. Uniaxial drawing of poly (vinyl alcohol)/graphene oxide nanocomposites. Carbon. 2014;70:38–45.
15. Morimune S, Nishino T, Goto T, et al. Ecological approach to graphene oxide reinforced poly (methyl methacrylate) nanocomposites. ACS Appl Mater Interfaces. 2012;4:3596–3601.
16. Zhao X, Zhang Q, Chen D, et al. Enhanced mechanical properties of graphene-based poly (vinyl alcohol) composites. Macromolecules. 2010;43: 2357–2363.
17. Sellam C, Zhai Z, Zahabi H, et al. High mechanical reinforcing efficiency of layered poly (vinyl alcohol) – graphene oxide nanocomposites. Nanocomposites. 2015;1:89–95.
18. Morimune-Moriya S, Ariyoshi M, Goto T, et al. Ultradrawing of poly (vinyl alcohol)/Graphene oxide nanocomposite fibers toward high mechanical performances. Compos Sci Technol. 2017;152: 159–164.
19. Shao-Yun F, Xi-Qiao F, Bernd L, et al. Effects of particle size, particle/matrix interface adhesion and particle loading on mechanical properties of particulate-polymer composites. Composites: Part B. 2008;39:933–961.
20. Alexandre M, Dubois P. Polymer-layered silicate nanocomposites: preparation, properties and uses of a new class of materials. Mater Sci Eng. 2000;28: 1–63.
21. Sumita M, Shizuma T, Miyasaka K, et al. Effect of reducible properties of temperature, rate of strain, and filler content on the tensile yield stress of nylon6 composites filled with ultrafine particles. J Macromol Sci Phys B. 1983;22:601–618.
22. Usuki A, Kawasumi M, Kojima Y, et al. Synthesis of nylon 6-clay hybrid. J Mater Res. 1993;8: 1179–1184.
23. Kojima Y, Usuki A, Kawasumi M, et al. Synthesis of nylon 6–clay hybrid by montmorillonite intercalated with ϵ-caprolactam. J Polym Sci A Polym Chem. 1993;31:983–986.
24. Halpin JC, Kardos JL. The Halpin–Tsai equations: a review. Polym Eng Sci. 1976;16:344–352.
25. Weon JI, Sue HJ. Effects of clay orientation and aspect ratio on mechanical behavior of nylon-6 nanocomposite. Polymer. 2005;46:6325–6334.
26. Abbasi SH, Hussein IA, Parvez MA. Nonisothermal crystallization kinetics study of LDPE/MWCNT nanocomposites: effect of aspect ratio and surface modification. J Appl Polym Sci. 2011;119:290–299.
27. Fischer B, Ziadeh M, Pfaff A, et al. Impact of large aspect ratio, shear-stiff, mica-like clay on mechanical behaviour of PMMA/clay nanocomposites. Polymer. 2012;53:3230–3237.
28. Kuvardina EV, Novokshonova LA, Lomakin SM, et al. Effect of the graphite nanoplatelet size on the mechanical, thermal, and electrical properties of polypropylene/exfoliated graphite nanocomposites. J Appl Polym Sci. 2013;128:1417–1424. DOI: 10.1002/APP.38237.
29. Guo J, Liu Y, Prada-Silvy R, et al. Aspect ratio effects of multi-walled carbon nanotubes on electrical, mechanical, and thermal properties of polycarbonate/mwcnt composites. J Polym Sci Part B: Polym Phys. 2014;52:73–83.
30. Nawaz K, Ayub M, Ul-Haq N, et al. Effects of selected size of graphene nanosheets on the mechanical properties of polyacrylonitrile polymer. Fibers Polym. 2014;15:2040–2044.
31. Greenfeld I, Wagner HD. Nanocomposite toughness, strength and stiffness: role of filler geometry. Nanocomposites. 2015;1:3–17.
32. Chong HM, Hinder SJ, Taylor AC. Graphene nanoplatelet-modified epoxy: effect of aspect ratio and surface functionality on mechanical properties and toughening mechanisms. J Mater Sci. 2016;51: 8764–8790.
33. Gao Y, Picot OT, Bilotti E, et al. Influence of filler size on the properties of poly (lactic acid) (PLA)/

graphene nanoplatelet (GNP) nanocomposites. Eur Polym J. 2017;86:117–131.
34. Begam T, Nagpal AK, Singhal R. A comparative study of swelling properties of hydrogels based on poly (acrylamide-*co*-methyl methacrylate) containing physical and chemical crosslinks. J Appl Polym Sci. 2003;89:779–786.
35. Young RJ, Kinloch IA, Gong L, et al. The mechanics of graphene nanocomposites: A review. Compos Sci Technol. 2012;72:1459–1476.
36. Young RJ, Liu M, Kinloch IA, et al. The mechanics of reinforcement of polymers by graphene nanoplatelets. Compos Sci Technol. 2018;72:110–116.
37. Qian D, Dickey EC, Andrews R, et al. Load transfer and deformation mechanisms in carbon nanotube-polystyrene composites. Appl Phys Lett. 2000;76:2868.
38. Mallick PK. Fiber-Reinforced Composites. New York: Marcel Dekker; 1993; p. 91–130.
39. Halpin JC, Thomas R. Ribbon reinforcement of composites. J Compos Mater. 1968;2:488–497.
40. Romanov V, Lomov SV, Verpoest I, et al. Interfiber stresses in composites with carbon nanotube grafted and coated fibers. Compos Sci Technol. 2015;114:79–86.
41. Olifrov LK, Kaloshkin SD, Zhang D. Study of thermal conductivity and stress-strain compression behavior of epoxy composites highly filled with Al and Al/f-MWCNT obtained by high-energy ball milling. Composites A. 2017;101:344–352.
42. Wang K, Chen L, Wu J, et al. Epoxy nanocomposites with highly exfoliated clay: Mechanical properties and fracture mechanisms. Macromolecules. 2005;38:788–800.
43. Su GM, Best K, Ranganathan T, et al. Nanoparticles for enhancing polymer adhesion. Macromolecules. 2011;44:5256–5261.
44. Krumova M, López D, Benavente R, et al. Effect of crosslinking on the mechanical and thermal properties of poly (vinyl alcohol). Polymer. 2000;41:9265–9272.
45. Liu H, Bandyopadhyay P, Kim NH, et al. Surface modified graphene oxide/poly (vinyl alcohol) composite for enhanced hydrogen gas barrier film. Polym Test. 2016;50:49–56.
46. Liu H, Liu C, Peng S, et al. Effect of polyethyleneimine modified graphene on the mechanical and water vapor barrier properties of methyl cellulose composite films. Carbohydr Polym. 2018;182:52–60.
47. Wolf C, Angellier-Coussy H, Gontard N, et al. How the shape of fillers affects the barrier properties of polymer/non-porous particles nanocomposites: a review. J Membr Sci. 2018;556:393–418.
48. Compton OC, Kim S, Pierre C, et al. Crumpled graphene nanosheets as highly effective barrier property enhancers. Adv Mater. 2010;22:4759–4763.
49. Tan B, Thomas NL. A review of the water barrier properties of polymer/clay and polymer/graphene nanocomposites. J Membr Sci. 2016;514:595–612.
50. Tan B, Thomas LN. Tortuosity model to predict the combined effects of crystallinity and nano-sized clay mineral on the water vapour barrier properties of polylactic acid. Appl Clay Sci. 2017;141:46–54.
51. Nielsen LE. Models for the permeability of filled polymer systems. J Macromol Sci A. 1967;1:929–984.
52. Cussler EL, Hughes SE, Ward WJ, et al. Barrier membranes. J Memb Sci. 1988;38:161–174.
53. Lai CL, Fu YJ, Chen JT, et al. Composite of cyclic olefin copolymer with low graphene content for transparent water-vapor-barrier films. Carbon. 2015;90:85–93.
54. Xu B, Zheng Q, Song Y, et al. Calculating barrier properties of polymer/clay nanocomposites: effects of clay layers. Polymer. 2006;47:2904–2910.
55. Alexandre B, Langevin D, Médéric P, et al. Water barrier properties of polyamide 12/montmorillonite nanocomposite membranes: structure and volume fraction effects. J Memb Sci. 2009;328:186–204.
56. Zhang Y, Liu Q, Zhang Q, et al. Gas barrier properties of natural rubber/kaolin composites prepared by melt blending. Appl Clay Sci. 2010;50:255–259.